Modelling gas cooling in Black Liquor Gasification

Lars Johansson, Lars Westerlund

Accepted Manuscript

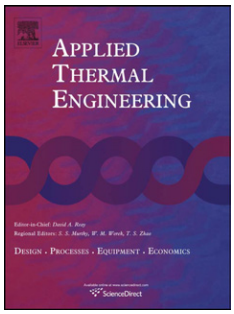

Title: Modelling gas cooling in Black Liquor Gasification

Authors: Lars Johansson, Lars Westerlund

PII: S1359-4311(11)00303-6

DOI: 10.1016/j.applthermaleng.2011.05.043

Reference: ATE 3590

To appear in: *Applied Thermal Engineering*

Received Date: 2 November 2010

Revised Date: 11 April 2011

Accepted Date: 31 May 2011

Please cite this article as: L. Johansson, L. Westerlund. Modelling gas cooling in Black Liquor Gasification, Applied Thermal Engineering (2011), doi: 10.1016/j.applthermaleng.2011.05.043

Modelling gas cooling in Black Liquor Gasification.

Lars Johansson & Lars Westerlund[1]

Division of Energy Engineering, Lulea University of Technology, S-971 87 Lulea, Sweden, Tel: +46 920 491223, Fax: +46 920 491047, e-mail: Lars.Westerlund@ltu.se

Abstract

Pressurized Entrained Flow High Temperature Black Liquor Gasification (PEHT-BLG) is a new technology not yet commercialized. The technology has the potential to improve the efficiency of energy and chemical recovery in the pulping industry. It also enables new processes, i.e. production of renewable motor-fuels from the syngas. The technology is not yet fully developed and interest in computer models for scale-up and optimization of the process in combination with experiments is favourable in the development process. A demonstration plant has been in operation since late 2005, in Pitea, Sweden. At Lulea University of Technology (LTU), a CFD model of a vertical tube in the counter current condenser has been developed using the commercial code FLUENT 6. The geometry is consistent with the demonstration plant and input data of the design has been used as boundary conditions for the model. The objective is to create a CFD model that can be used as a designing tool for the technology developer in future scale-up and for commercialized units. The model predicts the condensation process very well and shows that the major part of the condensation takes place in the first quarter of the tube under the given conditions. The heat transfer through the tube wall has been modelled based on results from the literature. The results show the importance of accurate heat transfer coefficients. Compared to designing data, the heat transfer through the wall and the condensate rate show good agreement. However, these results need to be validated against experimental data for different conditions.

Keywords

Condensation, Simulation, CFD, saturated.

Nomenclature

Roman letters

c_p	specific heat capacity (J/kg K)
h_{fg}	heat of vaporization (J/kg)
m	mass (kg)
$\dot{m}$	mass flow (kg/s)
m_f	mass fraction (-)
M	molecular weight (kg/mol)
N	number of mole
P	pressure (Pa)
$\dot{Q}$	heat transfer rate (W)
R	gas constant (J/kg K)
$\bar{R}$	universal gas constant (J/mole K)

[1] Corresponding author

T temperature (K)
V volume (m^3)
Z compressibility factor (-)

Greek letters
ϕ relative humidity (%)

Subscripts
cond condensate
cond1 transfer to gas phase
d droplet
i substance
mix mixture
ref reference value
sat saturated
w water vapour

Abbreviations

LTU	Lulea University of Technology
ETC	Energy Technology Centre
CFD	Computational Fluid Dynamics
DP-1	Demonstration Plant
PEHT-BLG	Pressurized Entrained-flow High Temperature Black Liquor Gasification

1. Introduction

Black liquor is a by-product in the papermaking process and an important liquid fuel in the pulp and paper industry. It is formed in the digester where organic material from the wood chips is dissolved in a cooking liquid, called white liquor, consisting mainly of sodium compounds. The black liquor is traditionally burnt in a recovery boiler where steam is generated for electricity generation and process steam. The remaining cooking chemicals are dissolved in water, forming green liquor that can be transformed into white liquor in the causticizing process.

Pressurized Entrained-flow High Temperature Black Liquor Gasification (PEHT-BLG) is a new technology not yet commercialized. The technology aims at improving aspects of the recovery process, chemical recovery and energy recovery. To deepen the insight into the process and prove reliability of the technology, Chemrec AB, has since late 2005 been operating a demonstration plant (DP-1), located at the Smurfit Kappa mill in conjunction with Energy Technology Centre (ETC) in Pitea, Sweden. The plant has a designing pressure of 30 bars (a) and a capacity of roughly 20 tonnes of black liquor dry solids per day.

1.1 Plant Description

Figure 1 illustrates the demonstration plant with three major components. In the reactor the black liquor is gasified at roughly 1000°C under sub-stoichiometric conditions using pure oxygen as reactant. The black liquor is fed through spray nozzles at the top of the reactor. A gas primarily consisting of CO, CO_2, H_2O and H_2 is formed together with smelt mainly consisting of Na_2CO_3 and Na_2S. In the quench, the lower part of the reactor, the gas flow and smelt is rapidly cooled. The smelt is separated from the gas flow through gravitation and

collected in the bottom of the quench where, dissolved with water, it forms green liquor. Through a conventional causticizing process the green liquor is transformed into white liquor.

Figure 1
Color for the web, Black and White in print

Downstream from the reactor the gas flow is cooled and water vapour is condensed. The counter current condenser consists of a bundle of tubes where the gas flows upwards on the inside of the tubes and the cooling water flows on the outside of the tubes in a zigzag pattern created by baffle plates, see Figure 2. The gas flow at the condenser inlet is almost saturated with water vapour and has a temperature of roughly 220 °C. The cooled synthesis gas can be utilized in different ways, for electricity production, automotive fuels or other chemicals.

CFD models concerning the upper part of the reactor were created by Marklund [1] and the lower part including the quench has been presented by Johansson & Westerlund [2]. This study focuses on a CFD model of the counter current condenser with the objective of creating a designing tool that can be used in future scale-ups towards commercialization or with alternative condenser geometries. Assuming similar conditions in all tubes, only one tube has been modelled. This decreases the computational time considerably.

Figure 2
Color for the web, Black and White in print

2. Theory

For water there is a definite relation between saturation pressure and saturation temperature. When the gas flow is cooled, the saturation pressure decreases. The reduced pressure is caused by transforming water vapour to liquid phase, i.e. condensation occurs.

Condensation models are not included in the commercial CFD code, and hence proper models describing the condensation have to be implemented. The condensation is treated using a Discrete Phase Model (DPM model), where very small droplets or aerosols are injected and used as condensational nucleus. Water vapour from the gas phase is converted to liquid state (condensed) and transported to the droplets. During passage through each computational cell with water content beyond saturation conditions, the droplets will grow in size due to condensation of water vapour. The latent heat released during condensation is transferred to the gas flow and cooled through convective heat transfer by the tube wall. In reality the gas has the lowest temperature close to the tube wall and condensation will therefore occur on the tube surface; a film of condensate will be built up and flows down the tube wall. Since the condensation occurs on discrete droplets implemented in the model, heat transfer through the tube wall is calculated for the continuous gas flow in the transport equations. The heat transfer with condensation is much larger than the characteristics of convection heat transfer without phase change. User-defined functions describing the heat flow have to be implemented.

In many cases it is assumed that the gas flow is an ideal mixture. The high pressure in the condenser (30 bar(a)), causes deviation from ideal conditions. If non-ideal conditions are assumed, the equation of state for a real mixture becomes [3],

$$P_{mix} \cdot V_{mix} = Z_{mix} \cdot N_{mix} \cdot \bar{R} \cdot T_{mix} = Z_{mix} \cdot m_{mix} \cdot R_{mix} \cdot T_{mix} \quad \textbf{(1)}$$

Where ($Z_{mix} = f\left(P_{mix}, T_{mix}\right)$) is the compressibility factor for the mixture and $\bar{R}$ is the universal gas constant (8314.51 J/mol·K). The mixture pressure (P_{mix}) is, according to Dalton's law, the sum of the components partial pressure ($P_i\left(T_{mix}, V_{mix}\right)$). (R_{mix}) is the gas constant for the gas mixture that is calculated using

$$R_{mix} = \sum m_{f,i} \cdot \frac{\bar{R}}{M_i} \quad \textbf{(2)}$$

The compressibility factor for water vapour is calculated using table values and Eq (1) and the compressibility factor for each other substances is calculated according to Lee-Kesler's generalized equation of state [4]

The compressibility factor for the mixture is determined using

$$Z_{mix} = \sum m_{f,i} \cdot Z_i \quad \textbf{(3)}$$

The relative humidity in the gas flow is per definition calculated from

$$\phi = \frac{P_w\left(T_{mix}\right)}{P_s\left(T_{mix}\right)} \quad \textbf{(4)}$$

$P_w\,(T_{mix})$ is the partial pressure for the water vapour and $P_s\,(T_{mix})$ is the saturation pressure for the water vapour at mixture temperature. $P_w(T_{mix})$ can be calculated using Eq. (1) for water and for the mixture in order to eliminate the volume from the expression. To simplify the expression, individual gas constants are replaced with the universal gas constant divided by molecular weight for water and mixture respectively

$$P_w(T_{mix}) = \frac{Z_w}{Z_{mix}} \cdot \frac{R_w}{R_{mix}} \cdot m_{f,w} \cdot P_{mix}(T_{mix}) = \frac{Z_w}{Z_{mix}} \cdot \frac{m_{f,w} \cdot P_{mix}(T_{mix})}{M_w \cdot \Sigma \frac{m_{f,i}}{M_i}} \quad \textbf{(5)}$$

Combining Eq. (4) and (5) yields a relative humidity according to

$$\phi = \frac{\frac{Z_w}{Z_{mix}} \cdot \frac{m_{f,w} \cdot P_{mix}(T_{mix})}{M_w \cdot \Sigma \frac{m_{f,i}}{M_i}}}{P_s\left(T_{mix}\right)} \quad \textbf{(6)}$$

A saturated condition corresponds to a relative humidity equal to unity. Condensation is initiated when the saturation pressure of the water vapour is reached. When the saturated mixture is cooled, the saturation pressure decreases and condensate is formed.

The maximum mass fraction of water in each cell can be expressed from Eq (6) as

$$m_{f,sat} = \frac{Z_{mix}}{Z_w} \cdot \frac{1.0 \cdot \mathrm{P}_s\left(\mathrm{T}_{mix}\right) \cdot \mathrm{M}_w \cdot \Sigma \frac{m_{f,i}}{M_i}}{P_{mix}(T_{mix})} \quad \textbf{(7)}$$

The condensate rate can be calculated using

$$\dot{m}_{cond} = \dot{m}_{mix} \cdot (m_{f,w} - m_{f,sat}) \quad \textbf{(8)}$$

The total mass flow $(\dot{m}_{mix})$ is determined by a mass balance for each cell. The energy released upon condensation will be added to the gas flow and lead to a temperature change within the gas flow. The temperature of the droplet is assumed uniform and set equal to the temperature of the gas flow in each computational cell. The energy transferred to the gas flow is calculated using

$$\dot{Q}_{cond1} = \dot{m}_{cond} \cdot c_{p,d} \cdot \left(T_d - T_{ref}\right) + \dot{m}_{cond} \cdot h_{fg} \quad \textbf{(9)}$$

where the first term corresponds to sensible heat and the second term corresponds to latent heat.

Heat transfer inside vertical tubes has been studied extensively in the literature. Maheshwari et. al. [5] presented a theoretical and experimental investigation of condensation for a wide range of Reynolds numbers. Maheshwari's model was also compared to other similar experiments carried out by Tanrikut and Yesin [6] and Siddique et al. [7]. The model results

showed good agreement with all the presented experiments. The model was based on a theoretical approach of heat and mass transfer at the gas/vapour boundary layer. Condensation in the presence of non-condensable gas has the main resistance to heat transfer in the gas/vapour boundary layer according to many studies. Forced convection conditions improve the statement further. The heat resistance of the condensate film diminishes due to rippling and waviness in the film. This improves convective heat transfer that increases the conduction in the film.

This paper focuses on the described experimental studies. The conditions in those studies are similar to the conditions used in this CFD model. The experiments carried out by Siddique were considered to have the best agreement with the conditions in this model. Siddique's experiments were carried out with the tube being cooled by water flowing inside a cooling jacket. A comparison between Siddique's experiments and the model described in this paper is presented in Table 1. The heat transfer coefficient used in the CFD model was calculated by a polynomial fitted curve to the experimental data, see Figure 3. Experimental and analytical studies performed by Lee et al. [8] shows similar behaviour.

Table 1. Comparison of characteristics (inlet conditions) between Siddique experiments and CFD model.

Characteristic	**Siddique's experiments**	**CFD model**
Tube length (m)	2.54	2.28
Inner diameter (m)	0.046	0.015
Non-condensable mass fraction (%)	22.4	25
Mixture Reynolds number	15139	16500

An experimental study performed by Henderson et al. [9] showed that condensation heat transfer results where similar comparing one single tube with a tube bundle of four vertical tubes. The results in this paper can therefore be used on a condenser consisting of several tubes.

3. Numerical simulations

The simulations were performed with the commercially available CFD-code, Fluent 6. The software includes a separate module for pre-processing. The above described models were implemented in the software through a total of 15 different subroutines. The basis of the code is a finite volume method, using an unstructured computational mesh and a segregated iterative solver based on the SIMPLEC algorithm [10]. For the continuous gas phase, the Reynolds Averaged Navier-Stokes equations (RANS) and energy equation are solved using an Eulerian description. The turbulent flow is modelled using the k-ε model with standard wall functions for turbulent flow [11].

The discrete droplets are tracked through the computational domain by integration of the momentum equation using a Lagrangian description. As the trajectory of a droplet is computed, the heat, mass and momentum gained or lost by the particle stream that follows the trajectory is calculated. These quantities are incorporated in the continuous phase calculations in the next iteration. If more than one droplet passes through a cell, changes in the source values are performed only once. For cells with no droplets and conditions above saturated state, a droplet is released in the centre of the computational cell.

The simulations were performed in a computational domain represented by an unstructured mesh consisting of 40,000 elements. Boundary layer from tube wall towards the centre of the tube was introduced.

The equations were solved using a 2nd order discretization scheme and double precision for numerical accuracy. The sum of the absolute residuals was used to estimate the iterative error. The residuals in the final solution were reduced by 3-4 orders of magnitude resulting in an estimated iterative error of 0.1%. [12]. The time needed for a convergent solution was approximately 2 days on a PC with a 3 GHz processor.

3.1 Operational and boundary conditions

The boundary conditions used in the simulations are presented in Table 2. The gas flow at the inlet is determined by specifying the mass flow, temperature and mass fractions of the different substances. At the tube outlet a constant static pressure profile was set, which means that the flow at the outlet was assumed to be fully developed. The total pressure in the computational domain was set at 30 bar (a). A linear temperature profile on the outside of the tube wall was specified corresponding to the heat-up of the cooling water flowing on the outside of the tube. At the top/bottom of the tube the values 25°C/68°C were used.

Table 2. Inlet boundary conditions for the gas flow used in the counter current condenser simulation.

Variable		**Unit**
Temperature	220	°C
Mass flow	$2.55 \cdot 10^{-3}$	kg/s
Mass fraction water vapour	75	% by weight
Mass fraction CO	9	% by weight
Mass fraction CO_2	13	% by weight
Mass fraction H_2	3	% by weight

The heat transfer rate from the gas to the tube wall is determined by the temperature difference between the gas and the inside of the tube, the area and the heat transfer coefficient. As mentioned in the theory section, a heat transfer coefficient profile has been set according to Figure 3.

Figure 3
Color for the web, Black and White in print

The injected droplets were specified with initial temperature corresponding to the temperature of the gas and an initial diameter of $1 \cdot 10^{-6}$ m. The amount of droplet trajectories in the DPM model was set at 146 in the computational domain.

4. Results

The compressibility factor (Z) for water vapour at saturated state is presented in Figure 4. The deviation from ideal conditions (Z=1) increases rapidly with temperature. Since water is the most important component in the calculations, it indicates that the compressibility factor needs to be implemented.

Figure 4
Black and White for the web and in print

Figure 5 shows the temperature and relative humidity of the gas flow along the tube with height 2.28 m and inner diameter $15 \cdot 10^{-3}$ m. The wall thickness of the stainless steel tube is $1.5 \cdot 10^{-3}$ m. For visibility reasons 2 paths were created, one in the centre of the tube (x0) and one path $3 \cdot 10^{-4}$ m from the tube wall (x1). The gas flow is cooled rapidly close to the inlet due to high heat transfer rates. Cooling through the tube wall gives the highest temperature in the centre of the tube. In the temperature plot (left), the outside tube temperature is also presented. The largest temperature change is in the first quarter of the tube. At the inlet, the temperature difference between the gas and the inside of the tube is approximately 150°C. 0.5 m downstream this difference has decreased to about 20°C. The condensation starts almost immediately since saturated conditions are reached. The cooling causes the relative humidity to be constant at 100% all the way through the tube. Since the condensation is controlled by saturated conditions, this should be expected, see Figure 5 (right).

Figure 5
Color for the web, Black and White in print

In Figure 6, temperature contour plots are displayed at the inlet, 0.3 m from the inlet and at the outlet of the tube. The highest temperature occurs at the centre of the tube and the gas flow is uniformly cooled towards the tube wall. At 0.3 m, the temperature difference between the centre and close to the wall can be seen. This deviation decreases closer to the outlet where it is almost vanished.

Figure 6
Color for the web, Black and White in print

The heat flux to the wall depends on the heat transfer coefficient and temperature difference between the gas flow and the tube wall. Both variables are large at the beginning of the tube, and hence the heat flux is large in this area. During condensation the latent heat is released and a large temperature difference is maintained, despite large heat fluxes to the wall, see Figure 7 (left). In the latter part of the tube, the heat flux to the wall reduces since the heat transfer coefficient and temperature difference decrease. In the first 0.5 m of the tube length, 97% of the total heat transfer rate is transferred.

Due to the large condensation rate, the mass fraction of water vapour decreases rapidly. After the first quarter of the tube, a large quantity of the water vapour has been condensed, see Figure 7 (right). 0.5 m from the inlet, 99% of the total condensation rate has taken place.

Figure 7
Color for the web, Black and White in print

Another important result from the simulation is shown in Figure 8. The velocity decreases from roughly 1.3 m/s at the inlet to 0.4 m/s due to the reduced mass flow from condensed water vapour. The Reynolds number decreases from 16,500 to 4,700 at the outlet.

Figure 8
Color for the web, Black and White in print

Figure 9 show a comparison between designing data for the condenser in DP-1 and results from the CFD simulations with default heat transfer coefficient in the CFD code (i.e. convection heat transfer without phase change.) and modified heat transfer coefficient described in the theory section. All other conditions are the same in the comparison. The condensate for the CFD models has been recalculated so that the condensate leaves the tube at the bottom. The left figure shows a complete energy balance with the different heat flows, and the corresponding values are presented graphically to the right. The first column in Figure 9 (right) shows the energy entering the tube ($\dot{Q}_{in}$). The supplied energy leaves the tube with the exhaust gas flow, through the wall and with the condensate.

Comparing the design data with the CFD model described in this paper shows good agreement. Roughly 70% of the supplied heat leaves the tube through the wall ($\dot{Q}_{wall}$), 28% leaves the tube with condensate ($\dot{Q}_{cond}$) and less than 2% of the energy leaves the tube with the exhaust gas flow ($\dot{Q}_{out}$). The last case, a CFD model with default heat transfer coefficient calculated without phase change shows a considerable deviation from the other two cases. The lower heat transfer coefficient leads to less energy through the tube wall and therefore less condensation, and hence an increased energy flow with the exhaust gas flow.

Figure 9
Color for the web, Black and White in print

5. Discussions and conclusions

The CFD model predicts the heat and mass transfer processes very well. The model also predicts a very rapid condensation. Under the given conditions only the first quarter of the condenser is actually active.

As shown above, the wall heat transfer coefficient is an important factor in the condenser model since it determines the cooling rate of the gas flow and therefore also the condensation that is influenced by the temperature. This indicates that further work on the heat transfer description within this model needs to be carried out in order to refine the model. The differences in principle between the experimental set up and the geometry in this model are the tube diameter, Reynolds number, the gas/condensate flow direction and pressure of the gas flow. An increased Reynolds number should increase the heat transfer coefficient. An increased tube diameter should have the opposite effect. The flow direction for gas/condensate was co-current in the experiments and counter-current in the model. The condensate film and the resistance to heat transfer will increase and reduce the heat transfer coefficient close to the inlet of the gas flow [13]. The influence on pressure is difficult to predict and should be established in future work, but the heat and mass transfer analogy can be applied even at high pressure [14].

A linear temperature profile on the outside of the tube was set in these calculations. Since the heat transfer rate changes along the tube, the temperature on the tube wall will also change accordingly. This will result in an increased condensation rate in the lower part of the tube. The total condensation rate will however stay the same.

Condensations on droplets instead of at the tube wall overestimate the condensation rate. In reality a larger part of the tube should be active. The model results show that only a minor part of condensation takes place more than two mm from the tube wall.

The interaction between the heat and mass transfer when water vapour condenses is difficult to predict, since a decreased temperature on the gas flow gives a lower saturation pressure and therefore an increased condensation rate. When condensation occurs, heat is released to the gas flow, which results in an increased temperature. This interacting phenomenon made simulations quite difficult and a convergent solution was difficult to reach in the beginning of the work. When the water vapour condenses and the energy is released, this results in large source terms and gradients in each computational cell. Also, since the condensation nuclei are modelled using a discrete phase model, a convergent solution for the continuous and discrete phase must be reached before the results can be analyzed.

Validation of CFD models is important to include in order to have confidence in the model output. In combination with experiments, computer models are a powerful tool in design and optimization. The demonstration plant has been in operation in periods a little more than a year. However, difficulties with measuring equipment in connection with the counter current condenser have complicated the collection of valid operational data that can be used for validation purposes. Further work will in the future include validation against experimental results. The results of this work show that the condenser during prescribed conditions is much too large, preferred data can be established with an apparatus much smaller than the one used in the demonstration plant, this will reduce the investment cost in a commercial plant.

Acknowledgements

This work has been carried out thanks to funding from the Swedish National Energy Administration (STEM), the Foundation for Strategic Environmental Research (MISTRA), Vattenfall AB, SCA Packaging AB, SmurfitKappa Packaging AB, Sveaskog AB, Södras Research Foundation, Chemrec AB and the County Administrative Board of Norrbotten. The work was part of the BLG programme coordinated by the Energy Technology Centre in Pitea, Sweden.

References

[1] Marklund M. (2006), Pressurized Entrained-flow High Temperature Black Liquor Gasification, PhD Thesis, Lulea University of Technology, Division of Fluid Mechanics, Lulea, Sweden.

[2] Johansson L. and Westerlund L. (2004), CFD modelling of the Quench in a Pressurized Entrained Flow Black Liquor Gasification Reactor. CHISA 2004, Czech Republic: 16th international congress of chemical and process engineering, pp. 11399-11409

[3] Cengel Y.A and Boles M.A. (2002), Thermodynamics-An Engineering Approach, McGraw Hill, New York, USA. ISBN: 0-07-238332-1.

[4] Lee B. I. and Kesler M. G. (1975), A generalized Thermodynamic correlation based on three- parameter corresponding states, AIChE J., vol. 21(3) pp. 510-527.

[5] Maheshwari N.K., Saha D., Sinha R.K. and Aritomi M. (2004), Investigation on condensation in presence of a noncondensable gas for a wide range of Reynolds number, Nuclear Engineering and Design, 227, pp. 219-238.

[6] Tanrikut A. and Yesin O. (1999). An experimental research on in-tube condensation in the presence of air. Proc. 2nd International Symposium on Two-phase Flow and Experimentation, Pisa, Italy, 23-26 May 1999, pp I367-I374.

[7] Siddique M., Golay M. W. and Kazimi M. S. (1993). Local heat transfer coefficients for forced convection condensation of steam in a vertical tube in the presence of a non-condensable gas. Nuclear Technology, 102(3), pp. 386-402.

[8] Lee K-Y and Kim M.H (2008), Effect of an interfacial shear stress on steam condensation in the presence of a noncondensable gas in a vertical tube. International Journal of Heat and Mass Transfer, 51, pp 5333-5343.

[9] Henderson G, Zhou W and Revankar S T (2010), Condensation in a vertical tube bundle passive condenser- Part 2: Complete condensation. International Journal of Heat and Mass Transfer, 53, pp 1156-1163.

[10] FLUENT (2004). Fluent 6 user guide, Sheffield Business Park, Sheffield, S9 1XU, UK.

[11] Wilcox D.C. (1993) Turbulence modelling for CFD, Griffin printing Glendale, USA.

[12] Ferziger P. and Peric M. (1999), Computational Methods for Fluid Dynamics, Berlin, Germany: Springer-Verlag, pp 314-319.

[13] Liao Y., Guentay S., Suckow D. and Dehbi A. (2009), Reflux condensation of flowing vapour and non-condensable gases counter-current to laminar liquid film in a vertical tube. Nuclear Engineering and Design, 239, pp 2409-2416.

[14] Kim J. W., Lee Y. G., Ahn H. K. and Park G. C. (2009), Condensation heat transfer characteristic in the presence of noncondensable gas on natural convection at high pressure. Nuclear Engineering and Design, 239, pp 688-698.

> Counter current condenser used in Black Liquor Gasification > A CFD model for simulation of a counter current condenser has been used > Simulations performed with a commercially available CFD-code Fluent 6 has been used.

Figure Captions for Manuscript *" Modelling gas cooling in Black Liquor Gasification".*

Figure 1. Schematic drawing of the PEHT-BLG process in Piteå, Sweden, (Chemrec AB).

Figure 2. Sketch showing the flow patterns in the counter current condenser.

Figure 3. Heat transfer coefficient profile on the inside of the tube wall.

Figure 4. Compressibility factor for saturated water vapour vs temperature.

Figure 5. Temperature (left) and relative humidity (right) of the gas flow along the tube.

Figure 6. Temperature plots at different cross sections along the tube.

Figure 7. Heat flux through the wall (left) and mass fraction of water vapour (right) along the tube.

Figure 8. Velocity of the gas flow along the tube.

Figure 9. Energy balance for one tube. Comparison between design data and simulation results for the condenser.